Theoretical study of spin-forbidden cooling transitions of indium hydride using *ab initio* methods*

Yun-Guang Zhang(张云光)†, Hua Zhang(张华), and Ge Dou(窦戈)

School of Science, Xi'an University of Posts and Telecommunications, Xi'an 710121, *China*

(Received 7 May 2017; revised manuscript received 5 June 2017; published online 18 July 2017)

The feasibility of spin-forbidden cooling of the InH molecule is investigated based on *ab initio* quantum chemistry calculations. The potential energy curves for the $X^1\Sigma^+_{0^+}$, $a^3\Pi_{0^-}$, $a^3\Pi_{0^+}$, $a^3\Pi_1$, $a^3\Pi_2$, $A^1\Pi_1$, $1^3\Sigma^+_{0^-}$, and $1^3\Sigma^+_1$ states of InH are obtained based on multi-reference configuration interaction plus the Davidson corrections method. The calculated spectroscopic constants are in good agreement with the available experimental data. In addition, the influences of the active space and spin–orbit coupling effects on the potential energy curves and spectroscopic constants are also studied. For R_e of $a^3\Pi_{0^-}$, $a^3\Pi_{0^+}$, $a^3\Pi_1$, and $a^3\Pi_2$ states, the error from large active space is small. The potential energy curve of the $A^1\Pi_1$ state is not smooth for small active space. The spin–orbit coupling effects have great influences on the potential well depth and equilibrium internuclear distance of the $A^1\Pi$ state. The Franck–Condon factors and radiative lifetimes are obtained on the basis of the transition dipole moments of the $a^3\Pi_{0^+} \rightarrow X^1\Sigma^+_{0^+}$, $a^3\Pi_1 \rightarrow X^1\Sigma^+_{0^+}$, and $A^1\Pi_1 \rightarrow X^1\Sigma^+_{0^+}$ transitions. Our calculation indicates that the $a^3\Pi_1\,(v'=0) \rightarrow X^1\Sigma^+_{0^+}\,(v=0)$ transition provides a highly diagonally distributed Franck–Condon factor and a short radiative lifetime for the $a^3\Pi_1$ state, which can ensure rapid and efficient laser cooling of InH. The proposed laser drives $a^3\Pi_1 \rightarrow X^1\Sigma^+_{0^+}$ transitions by using three wavelengths.

Keywords: spectroscopic constants, Franck–Condon factors, transition dipole moments, spin-forbidden cooling transition

PACS: 31.15.A–, 37.10.Mn, 87.80.Cc **DOI:** 10.1088/1674-1056/26/9/093101

1. Introduction

Laser cooling to create unique ultracold molecules has aroused considerable interest[1–4] because of their promising applications, for example, new platforms for quantum computing,[5] quantum controlled chemistry,[6,7] precision measurement,[8–10] and quantum simulation.[11,12] Naturally the search for potential laser cooling candidates is attracting more and more interest. The direct cooling of a diatomic molecule to the order of microkelvin was firstly achieved in SrF using only three laser beams in 2010,[1] which has initiated a search for more molecules that may be controlled in a similar way. Later, successful laser cooling experiments have been performed for YO,[13] CaF,[14] BH,[15] and BaH.[16] Besides the experimental studies on laser cooling candidates, theoretical optical schemes have been suggested for MgCl,[17] MgBr,[17] BeI,[18] MgI,[18] BeCl,[19] BeBr,[19] BeF,[20] MgF,[21] LiBe,[22] as well as for MH (M = Be, Mg, Ca, Sr, and Ba).[23] According to the previous investigations, the Doppler laser-cooling process must meet these significant criteria: highly diagonal Franck–Condon factors (FCFs), limiting number of lasers required to keep the molecule in a closed-loop cooling cycle, and short radiative lifetime τ describing rapid laser cooling. In theory, most of the studies have focused on spin-allowed transitions ($A^2\Pi - X^2\Sigma^+$ or $A^1\Pi - X^1\Sigma^+$). While Kobayashi *et al*. experimentally confirmed that the spin-forbidden transition $B^3\Pi \rightarrow X^1\Sigma^+$ is well suited for laser cooling of the KRb[3] molecule in 2014. In addition, the laser cooling scheme using the spin-forbidden transition has also been theoretically studied on AlF,[24] BBr,[25] BCl,[25] and LiRb.[26] These results open the door to all-optical production of polar molecules at sub-microkelvin temperatures and highlight the possibility of finding similar molecules that can be laser cooled.

Indium monohalides have been attracting interest for a long time because of their applications in the etching process of semiconductor devices. Experimental studies and theoretical calculations have been performed for InH over the past several decades. In 1939, the electronic spectrum of InH was reported, and bands of two transitions (i.e., Σ–Σ and Π–Σ) were rotationally analyzed by Grundström.[27,28] Garton[29] presented a band system in the wavelength region of 233–250 nm in 1951, but the system was not assigned. Subsequently, Neuhaus *et al.*[30,31] measured the $A^1\Pi$–$X^1\Sigma^+$ and $a^3\Pi$–$X^1\Sigma^+$ absorption spectra of InH and obtained the spectroscopic constants. Ginter[32–34] fitted the Rydberg–Klein–Rees curves of $X^1\Sigma^+_{0^+}$, $a^3\Pi_{0^+}$, and $a^3\Pi_1$ states, and found $a^3\Pi_{0^+}$–$X^1\Sigma^+_{0^+}$ and $a^3\Pi_1$–$X^1\Sigma^+_{0^+}$ transitions. Ogilvie[35] later determined the potential energy and coefficients of radial func-

*Project supported by the National Natural Science Foundation of China (Grant Nos. 11104217 and 11402199) and the Program for New Scientific and Technological Star of Shaanxi Province, China (Grant No. 2012KJXX-39).

†Corresponding author. E-mail: zygsr2010@163.com

© 2017 Chinese Physical Society and IOP Publishing Ltd

tions of InH in the ground state $X^1\Sigma^+$ from the rovibrational spectrum. In 1993, Rajamanickam *et al.*[36] refitted the Rydberg–Klein–Rees curves of the $X^1\Sigma^+_{0^+}$ and $a^3\Pi_1$ states, and obtained the FCFs of the $a^3\Pi_1$–$X^1\Sigma^+_{0^+}$ system. In 2003, Zou *et al.*[37] investigated the potential energy curves (PECs) and the spectroscopic constants of the $X^1\Sigma^+_{0^+}$, $a^3\Pi_{0^-}$, $a^3\Pi_{0^+}$, $a^3\Pi_1$, $a^3\Pi_2$, and $A^1\Pi_1$ states using the second order CI and relativistic CI methods, and predicted the transition properties of the excited states. Most recently, analytic potential energy functions were computed for the $X^1\Sigma^+_{0^+}$ and $a^3\Pi_{0^+}$ states of InH using a dict-potenial-fit analysis by Alireza Shayesteh *et al.*[38] However, a systematic study of laser cooling of InH is, to the best of our knowledge, is so far unavailable. We focus in the present work on the theoretical study of the laser cooling of InH molecule employing different active spaces. The electronic structures and transition properties associated with the laser cooling of InH are calculated, including FCFs, transition dipole moments (TDMs), and radiative lifetimes of the $A^1\Pi_1 \rightarrow X^1\Sigma^+_{0^+}$, $a^3\Pi_{0^+} \rightarrow X^1\Sigma^+_{0^+}$, and $a^3\Pi_1 \rightarrow X^1\Sigma^+_{0^+}$ transitions of the InH molecule. A scheme for a feasible laser cooling cycle of InH is designed briefly.

Section 2 describes the *ab initio* methods and basis sets used in the calculations of the electronic states of InH. Section 3 presents the results and discussion of the data, outlining laser cooling schemes for InH. We draw a conclusion for this work in Section 4.

2. Computational details

All the *ab initio* calculations are performed using the MOLPRO package.[39] The electronic states $X^1\Sigma^+$, $a^3\Pi$, $A^1\Pi$, and $1^3\Sigma^+$ of InH molecule have been calculated with multi-reference configuration interaction (MRCI) plus Davidson corrections (MRCI+Q) method,[40–42] which is based on the complete active space self-consistent-field (CASSCF)[43,44] wave functions. Scalar relativistic effects are included throughout the Douglas–Kroll–Hess[45,46] transformation of the relativistic Hamiltonian. The spin–orbit coupling (SOC) effects are also taken into account following the MRCI+Q calculations for the InH molecule. Due to the limitation of the symmetry of the MOLPRO program package, the computations are performed within the C_{2v} point group symmetry, which has four irreducible representations (A_1, B_1, B_2, and A_2). In the CASSCF and MRCI+Q calculations, 23 or 14 molecular orbitals are chosen as the active space, including eleven or seven a_1, five or three b_1, five or three b_2, and two or one a_2 symmetry. Fourteen electrons are distributed in (11552) or (7331) active space. The aug-ccpV5Z (AV5Z) basis set is used for the H atom. For the In atom, we take the small-core scalar relativistic effective core potential (ECP) ECP28MDF-AV5Z with the corresponding valence basis sets.

The nuclear Schrödinger equation is solved using the LEVEL 8.2 program[47] to evaluate the spectroscopic constants, including the equilibrium bond length (R_e), harmonic and inharmonic vibrational constants (ω_e and $\omega_e x_e$), rotational constant (B_e), adiabatic relative electronic energy referred to the ground state (T_e), and dissociation energy (D_e) for the ground and the low-lying states of InH. The $1^3\Sigma^+$ states are repulsive; therefore, they are not discussed in detail. All PECs are calculated with an interval of 0.05 Å over the distance from 1.1 Å to 9 Å. To obtain accurate results, the interval value is reduced to 0.02 Å near the equilibrium bond distance. The permanent dipole moments (PDMs) and TDMs are computed by the MRCI+Q method. The FCFs and radiative lifetimes of the various vibrational levels for $a^3\Pi_{0^+}$–$X^1\Sigma^+_{0^+}$, $a^3\Pi_1$–$X^1\Sigma^+_{0^+}$ and $A^1\Pi_1$–$X^1\Sigma^+_{0^+}$ transitions of InH are also determined from the LEVEL 8.2 program with the PECs and TDMs of different electronic states.

3. Results and discussion

3.1. PECs and spectroscopic constants

In order to understand the possibility of laser-cooling InH molecule, we investigate the $X^1\Sigma^+$, $a^3\Pi$, $A^1\Pi$, and $1^3\Sigma^+$ states of InH with the lowest dissociation channel $In(^2P) + H(^2S)$ at the MRCI+Q level. Because InH is a heavy nuclear molecule, the SOC effects are considered in calculations. The dissociation limit $In(^2P) + H(^2S)$ splits into two asymptotes, namely, $In(^2P_{1/2}) + H(^2S_{1/2})$ and $In(^2P_{3/2}) + H(^2S_{1/2})$. These two dissociation limits produce eight Ω states. The PECs for the $X^1\Sigma^+_{0^+}$, $a^3\Pi_{0^-}$, $a^3\Pi_{0^+}$, $a^3\Pi_1$, $a^3\Pi_2$, $A^1\Pi_1$, $1^3\Sigma^+_{0^-}$, and $1^3\Sigma^+_1$ states of InH are plotted in Fig. 1. The corresponding spectroscopic constants are tabulated in Table 1 along with available experimental data[48] for comparison.

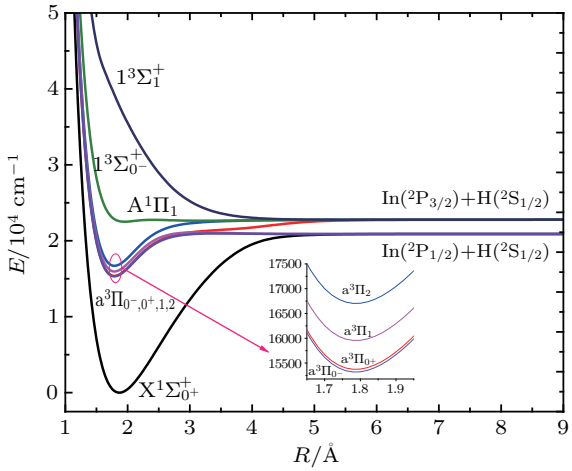


Fig. 1. (color online) The PECs including Ω splitting of the low-lying electronic states of InH molecule.

Table 1. Spectroscopic constants for InH molecule at the MRCI+Q level.

State	R_e/Å	ω_e/cm^{-1}	$\omega_e x_e$/cm^{-1}	B_e/cm^{-1}	D_e/cm^{-1}	T_e/cm^{-1}	
$X^1\Sigma^+$ (11552)	1.8689	1439.7738	21.6442	4.8298	22101.832	0	
$X^1\Sigma^+$ (7331)	1.8704	1445.2975	21.8883	4.8220	22307.502	0	
$X^1\Sigma^+_{0^+}$ (11552)	1.8683	1440.2563	21.7452	4.8332	20.897.656	0	
$X^1\Sigma^+_{0^+}$ (7331)	1.8698	1445.8084	21.9889	4.8254	221098.487	0	
	1.8380	1476.04	25.61	4.9945	–	0	Exp.[48]
$a^3\Pi$ (11552)	1.7871	1497.3089	61.1443	5.3009	6133.797	15968.357	
$a^3\Pi$ (7331)	1.7927	1495.8465	63.6157	5.2703	6004.749	16302.792	
$a^3\Pi_{0^-}$ (11552)	1.7871	1496.8152	61.4561	5.3011	5578.085	15319.772	
$a^3\Pi_{0^-}$ (7331)	1.7927	1494.6673	63.7522	5.2703	5449.844	15648.659	
	1.776	–	–	5.349	–	–	Exp.[48]
$a^3\Pi_{0^+}$ (11552)	1.7871	1499.9805	60.5903	5.3001	7397.657	15374.570	
$a^3\Pi_{0^+}$ (7331)	1.7928	1498.2571	62.9870	5.2692	7273.449	15706.774	
	1.7794	1458.57	61.03	5.329	–	16278.15	Exp.[48]
$a^3\Pi_1$ (11552)	1.7881	1481.8469	45.2605	5.2920	4940.912	15956.470	
$a^3\Pi_1$ (7331)	1.7937	1475.4610	39.2136	5.2419	4814.284	16284.843	
	1.7678	1415.11	43.55	5.3996	–	16941.61	Exp.[48]
$a^3\Pi_2$ (11552)	1.7878	1511.6053	70.9483	5.2936	6069.273	16703.217	
$a^3\Pi_2$ (7331)	1.7934	1505.7961	71.2684	5.2626	5941.838	17037.959	
	1.753	–	–	5.489	–	–	Exp.[48]
$A^1\Pi$ (11552)							
First well	1.9527	–	–	–	-308.101	22410.331	
Second well	3.9783	53.5320	–	0.8459	44.360	22057.855	
$A^1\Pi$ (7331)							
First well	1.9541	–	–	–	–262.128	22569.823	
Ssecond well	3.9887	–	–	–	66.943	22240.940	
$A^1\Pi_1$ (11552)							
First well	1.9504	456.0359	200.5752	4.4356	261.322	22511.153	
Second well	3.1884	83.5779	14.3462	1.6598	126.628	22646.205	
$A^1\Pi_1$ (7331)							
First well	1.9518	418.8749	–	4.4293	308.908	22671.012	
Second well	3.1942	–	–	–	137.920	22842.542	

As can be seen from Table 1, the influence of the SOC effect on the spectroscopic constants for the ground state seems to be weak. For example, the vibrational frequency ω_e and anharmonic vibrational constants $\omega_e x_e$ of the $X^1\Sigma^+$ state are computed to be 1439.7738 cm^{-1} and 21.6642 cm^{-1}, which differ from the values of $X^1\Sigma^+_{0^+}$ by 0.4825 cm^{-1} and 0.101 cm^{-1}, respectively. The SOC effects are considered in the calculations for the $a^3\Pi$ state, which splits into four Ω states ($a^3\Pi_{0^-}$, $a^3\Pi_{0^+}$, $a^3\Pi_1$, and $a^3\Pi_2$). In addition, to obtain accurate results, the effects of the active space are also considered for the InH molecule. The study of spectroscopic constants mainly focuses on two active spaces (11552) and (7331). The active space has a weak influence on the spectroscopic constants of the $X^1\Sigma^+$ and $a^3\Pi$ states. For the $X^1\Sigma^+$ state, the values of ω_e and B_e from active spaces (11552) and (7331) are very close. For the $a^3\Pi$ state, the calculated ω_e and B_e results for active space (11552) are only 1.462 cm^{-1} and 0.030 cm^{-1} larger than those for active space (7331). Meanwhile, the effects of the different active spaces (11552) and (7331) on the spectroscopic constants of the Ω sub-states $X^1\Sigma^+_{0^+}$, $a^3\Pi_{0^-}$, $a^3\Pi_{0^+}$, $a^3\Pi_1$, and $a^3\Pi_2$ are considered. The results indicate that the effects of the active space on the spectroscopic constants of these states are insignificant. The ω_e values of the $a^3\Pi_{0^-}$ and $a^3\Pi_2$ sub-states for active space (11552) are 1496.8152 cm^{-1} and 1511.6053 cm^{-1}, which are in excellent agreement with the values of 1494.6673 cm^{-1} and 1505.7961 cm^{-1} for active space (7331). Our values of $\omega_e x_e$ of the $a^3\Pi_{0^-}$ and $a^3\Pi_2$ states for active space (11552) are slightly larger than those for active space (7331). Thus the following analyses mainly focus on the results on the basis of active space (11552). For $X^1\Sigma^+_{0^+}$, $a^3\Pi_{0^+}$, and $a^3\Pi_1$ states, the equilibrium bond distances R_e are calculated to be 1.8683 Å, 1.7871 Å, and 1.7881 Å, and the corresponding percentage errors are only 1.65%, 0.43%, and 1.15% with respect to the experimental values, respectively; the differences in the rotational constant B_e for the three states are 0.1613 cm^{-1}, 0.0289 cm^{-1}, 0.1076 cm^{-1}, respectively; and notably, the calculated T_e for the $X^1\Sigma^+_{0^+}$, $a^3\Pi_{0^+}$, and $a^3\Pi_1$ states are 0, 15374.570 cm^{-1}, and 15956.470 cm^{-1}, which match well with the experimental values of 0, 16278.15 cm^{-1}, and 16941.61 cm^{-1}. The spectroscopic constants for the $a^3\Pi_{0^-}$ and $a^3\Pi_2$ states are

also predicted: $\omega_e = 1496.8152$ cm^{-1} and 1511.6053 cm^{-1}, $\omega_e x_e = 61.4561$ cm^{-1} and 70.9483 cm^{-1}. However, the equilibrium distances R_e of the $X^1\Sigma^+_{0^+}$, $a^3\Pi_{0^-}$, $a^3\Pi_{0^+}$, $a^3\Pi_1$, and $a^3\Pi_2$ states for active space (11552) are respectively 1.8683 Å, 1.7871 Å, 1.7871 Å, 1.7881 Å, and 1.7878 Å, which are closer to the experimental data[48] than those for active space (7331). Because the equilibrium separation has an important influence on FCFs, the results from active space (11552) are more suitable to evaluate the effect of laser cooling.

As shown in Fig. 2, the influence of the SOC effects and active space on the PECs of the $A^1\Pi$ state is significant. The dissociation limit of the Ω state is greater than that of the Λ–S state. The PECs of the active space (11552) are smoother than those of the active space (7331), which implies that active space (11552) is more conducive to research laser cooling. The PECs of the $A^1\Pi$ and $A^1\Pi_1$ states have two potential wells. Moreover, the second potential well and the second equilibrium bond length have a distinct change with the SOC effects. It can be seen from Table 1, for the $A^1\Pi$ state, the second well is placed at 22057.855 cm^{-1} above the ground state and the depth is 44.360 cm^{-1}. For the $A^1\Pi_1$ state, the second well is placed at 22646.205 cm^{-1} above the ground state, and the depth is 126.628 cm^{-1}. The equilibrium internuclear distances of the second potential well for the $A^1\Pi$ and $A^1\Pi_1$ states are 3.9783 cm^{-1} and 3.1884 cm^{-1}, respectively. In addition, the ω_e, $\omega_e x_e$, and B_e of the first potential well and $\omega_e x_e$ of the second potential well cannot be obtained because the $A^1\Pi$ state has two so shallow potential wells that there is only one vibrational level in them. So no experimental data were available for the $A^1\Pi$ and $A^1\Pi_1$ states before.

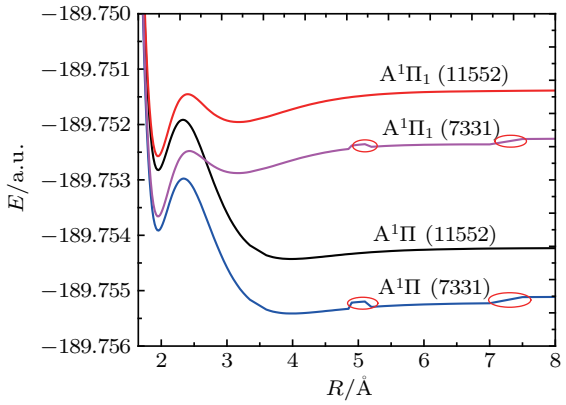


Fig. 2. (color online) The PECs for the $A^1\Pi$ and $A^1\Pi_1$ states based on two different active spaces.

3.2. PDMs and TDMs

The PDMs for the $X^1\Sigma^+$, $X^1\Sigma^+_{0^+}$, $A^1\Pi$, $A^1\Pi_1$, $a^3\Pi$, $a^3\Pi_{0^-}$, $a^3\Pi_{0^+}$, $a^3\Pi_1$, and $a^3\Pi_2$ states and the TDMs for the $a^3\Pi_{0^+} \rightarrow X^1\Sigma^+_{0^+}$, $a^3\Pi_1 \rightarrow X^1\Sigma^+_{0^+}$, and $A^1\Pi_1 \rightarrow X^1\Sigma^+_{0^+}$ transitions as a function of the internuclear distance at the MRCI+Q level of InH are plotted in Figs. 3 and 4, respectively. Figure 3(a) exhibits that the maxima of PDMs of the $X^1\Sigma^+$ and $X^1\Sigma^+_{0^+}$ states are much larger than those of the $A^1\Pi$ and $A^1\Pi_1$ states, and the reason is that the potential well of the ground state is the deepest. The PDMs of the $X^1\Sigma^+$ and $X^1\Sigma^+_{0^+}$ states exhibit a similar behavior with respect to the internuclear distance, the magnitudes of the PDMs reach a maximum ($X^1\Sigma^+$: 1.86080 a.u. and $X^1\Sigma^+_{0^+}$: 1.84172 a.u.) and drop thereafter. The PDMs of the $A^1\Pi$ and $A^1\Pi_1$ states also demonstrate a similar behavior, the magnitude increases as the internuclear distance increases, reaching a maximum ($A^1\Pi$: 0.14758 a.u. and $A^1\Pi_1$: 0.14762 a.u.). There are minima of PDMs of the $A^1\Pi$ and $A^1\Pi_1$ states at 2.6 Å and 2.55 Å, respectively. Figure 3(b) shows that the PDMs for the $a^3\Pi$, $a^3\Pi_{0^-}$, $a^3\Pi_{0^+}$, $a^3\Pi_1$, and $a^3\Pi_2$ states at R_e are 0.23545 a.u., 0.23496 a.u., 0.23506 a.u., 0.23426 a.u., and 0.23545 a.u., respectively. The PDM shows a linear behavior up to approximately 2.00 Å for the $a^3\Pi$, $a^3\Pi_{0^-}$, $a^3\Pi_{0^+}$, $a^3\Pi_1$, and $a^3\Pi_2$ states and then drops, and the maxima of PDMs are 0.27961 a.u., 0.27831 a.u., 0.28025 a.u., 0.27589 a.u., and 0.27961 a.u., respectively. The PDMs of the $a^3\Pi$ and $a^3\Pi_2$ states overlap. The PDM of the $a^3\Pi_{0^+}$ state increases from 3.2 Å to 4.4 Å and then declines. The PDMs of these states all tend to zero at about 5.3 Å.

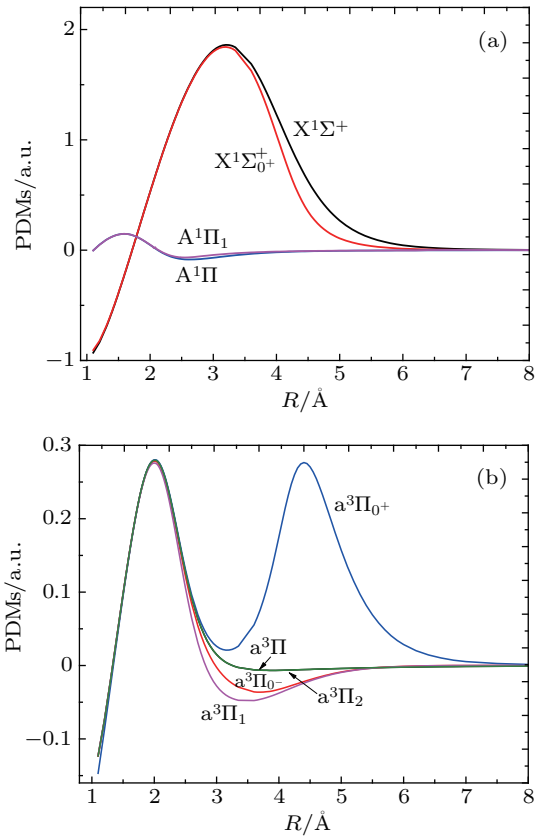


Fig. 3. (color online) The PDMs of (a) $X^1\Sigma^+$, $X^1\Sigma^+_{0^+}$, $A^1\Pi$, $A^1\Pi_1$, and (b) $a^3\Pi$, $a^3\Pi_{0^-}$, $a^3\Pi_{0^+}$, $a^3\Pi_1$, $a^3\Pi_2$ states of InH molecule.

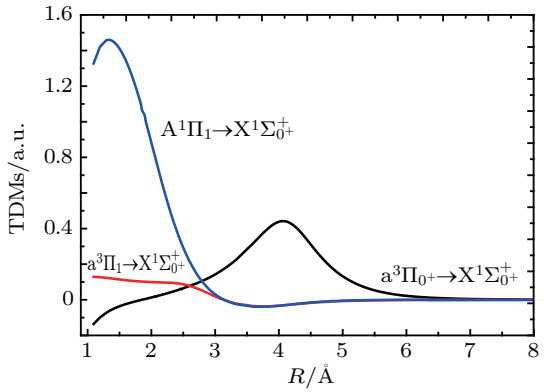


Fig. 4. (color online) The TDMs of the $A^1\Pi_1 \rightarrow X^1\Sigma^+_{0^+}$, $a^3\Pi_{0^+} \rightarrow X^1\Sigma^+_{0^+}$, and $a^3\Pi_1 \rightarrow X^1\Sigma^+_{0^+}$ transitions of InH molecule.

Three transitions $a^3\Pi_{0^+} \rightarrow X^1\Sigma^+_{0^+}$, $a^3\Pi_1 \rightarrow X^1\Sigma^+_{0^+}$, and $A^1\Pi_1 \rightarrow X^1\Sigma^+_{0^+}$ are calculated in the present work. We omit the $a^3\Pi_{0^-} \rightarrow X^1\Sigma^+_{0^+}$ and $a^3\Pi_2 \rightarrow X^1\Sigma^+_{0^+}$ transitions because they are forbidden according to the selection rules. Figure 4 shows that the TDMs of the $A^1\Pi_1 \rightarrow X^1\Sigma^+_{0^+}$ and $a^3\Pi_{0^+} \rightarrow X^1\Sigma^+_{0^+}$ transitions tend to zero at large distances owing to the orbit-forbidden transitions at the atomic limits from $In(^2P_{1/2})$ to $In(^2P_{3/2})$. Nevertheless, the TDM of the $a^3\Pi_1 \rightarrow X^1\Sigma^+_{0^+}$ transition tends to zero at large distances because the dissociation limits of the $a^3\Pi_1$ and $X^1\Sigma^+_{0^+}$ states are the same. That is, there is no transition at the atomic limits from $In(^2P_{1/2})$ to $In(^2P_{1/2})$. The maxima of TDMs for these three transitions are less than 1.50 a.u., and the $a^3\Pi_{0^+} \rightarrow X^1\Sigma^+_{0^+}$ and $a^3\Pi_1 \rightarrow X^1\Sigma^+_{0^+}$ transitions are much weaker than the $A^1\Pi_1 \rightarrow X^1\Sigma^+_{0^+}$ transition because the $a^3\Pi_{0^-} \rightarrow X^1\Sigma^+_{0^+}$ and $a^3\Pi_2 \rightarrow X^1\Sigma^+_{0^+}$ transitions are spin-forbidden. The TDMs for the $A^1\Pi_1 \rightarrow X^1\Sigma^+_{0^+}$ and $a^3\Pi_{0^+} \rightarrow X^1\Sigma^+_{0^+}$ transitions increase as the internuclear distance R increases, reach maxima (1.46031 a.u. and 0.44178 a.u.), and drop thereafter. The TDM for the $a^3\Pi_1 \rightarrow X^1\Sigma^+_{0^+}$ transition is reducing. Finally, the TDMs of InH all tend to zero at around 6.6 Å.

3.3. FCFs and spontaneous radiative lifetimes

The calculated FCFs can be used to describe the overlap of the vibrational wave functions for the cooling transition. To demonstrate the distributions of FCFs ($q_{v'v}$) for the different vibrational states of $a^3\Pi_{0^+}(v') \rightarrow X^1\Sigma^+_{0^+}(v)$, $a^3\Pi_1(v') \rightarrow X^1\Sigma^+_{0^+}(v)$, and $A^1\Pi_1(v') \rightarrow X^1\Sigma^+_{0^+}(v)$ transitions, we have sketched all possible transitions between $0 \le v \le 3$ and $0 \le v' \le 1$ in Table 2 to show the obvious characteristic that the transitions of $\Delta v = v - v' = 0$ have the largest probabilities. Highly diagonal FCFs obey the first criterion to be a potential laser-cooling candidate which could limit the number of lasers required to keep the molecule in a closed-loop cooling cycle. Unfortunately, the FCFs of the $A^1\Pi_1 \rightarrow X^1\Sigma^+_{0^+}$ ($q_{00} = 0.2350$) transition are very small. Therefore, it is not possible to cool the InH molecule based on the spin-allowed transition.

Table 2. The calculated Franck–Condon factors $q_{v'v}$, wavelength $\lambda_{vv'}$, $A_{v'v}$, and estimated spontaneous radiative lifetimes τ.

Transition	q_{00}	q_{01}	q_{02}	q_{03}	λ_{00}/nm	λ_{10}/nm	λ_{21}/nm	$A_{v'v}/s^{-1}$	$\tau(=1/A'_v)$/s
	q_{10}	q_{11}	q_{12}	q_{13}					
$a^3\Pi_{0^+} \rightarrow X^1\Sigma^+_{0^+}$	0.9100	0.0726	0.0147	0.0021	650.1215	715.2175	713.9894	5.0893×10^3	1.9649×10^{-4}
	0.0880	0.8132	0.0626	0.0304					
$a^3\Pi_1 \rightarrow X^1\Sigma^+_{0^+}$	0.9151	0.0679	0.0145	0.0020	626.6523	686.9154	686.4697	9.8821×10^5	1.0119×10^{-6}
	0.0822	0.8293	0.0528	0.0305					
$A^1\Pi_1 \rightarrow X^1\Sigma^+_{0^+}$	0.2350	0.2043	0.1733	0.1024					
	0.1442	0.1914	0.0989	0.1107					

As listed in Table 2, the present FCFs of the $a^3\Pi_{0^+}(v' = 0) \rightarrow X^1\Sigma^+_{0^+}(v = 0)$ and $a^3\Pi_1(v' = 0) \rightarrow X^1\Sigma^+_{0^+}(v = 0)$ transitions reach 0.9100 and 0.9151, respectively. The $A^1\Pi_1$ state is prohibitive to the cooling cycle because of the small diagonal FCF ($q_{00} = 0.0235$) for the $A^1\Pi_1 \rightarrow X^1\Sigma^+_{0^+}$ transition. By comparing with other molecules, our calculated value is slightly larger than that predicted for BeF ($q_{00} = 0.897$),[20] LiRb ($q_{00} = 0.872$),[26] and smaller than that for SrF ($q_{00} = 0.98$).[1] Therefore, the FCFs of InH are sufficiently large for laser cooling. Aside from the large diagonal FCFs, short spontaneous radiative lifetime τ (10^{-8}–10^{-5} s)[23] is another criterion for the laser cooling of molecules, which can provide a significant rate of rapid cycling. The corresponding computed radiative lifetimes are collected in Table 2. The spontaneous radiative lifetime τ of the $a^3\Pi_{0^+} \rightarrow X^1\Sigma^+_{0^+}$ transition is 1.9649×10^{-4} s, which is too long. Yet, the spontaneous radiative lifetime τ of the $a^3\Pi_1 \rightarrow X^1\Sigma^+_{0^+}$ transition is 1.0119×10^{-6} s, which is suitable for laser cooling InH molecule.

We also evaluate the branching ratios $R_{v'v}$, which can be expressed as $R_{v'v} = A_{v'v}/\sum_v A_{v'v}$. Branching ratios of the diagonal terms $R_{00} = 0.9357$ and $R_{11} = 0.8403$ for the $a^3\Pi_1(v') \rightarrow X^1\Sigma^+_{0^+}(v)$ transition are obtained; and branching ratios of the off-diagonal terms $R_{01} = 5.78\times10^{-2}$, $R_{02} = 6.37\times10^{-3}$, $R_{03} = 1.10\times10^{-4}$, $R_{10} = 9.26\times10^{-2}$, $R_{12} = 6.56\times10^{-2}$, and $R_{13} = 1.09\times10^{-3}$ are also calculated. Due to the branching to $v \ge 3$ states of InH are expressed as $R_{03^+} < 3\times10^{-5}$, we propose a cyclic system with three lasers

involving $v = 0$, 1, 2, 3 of the $X^1\Sigma^+_{0^+}$ state and $v' = 0$, 1 of the $a^3\Pi_1$ state based on the calculated $R_{v'v}$. The laser driven transitions (solid red) and spontaneous decays (dash line) in the proposed scheme are plotted in Fig 5. The calculated wavelength of the principal laser-driven cycling of the $a^3\Pi_1(v' = 0) \rightarrow X^1\Sigma^+_{0^+}(v = 0)$ transition is the main pump in Fig. 5, whose wavelength λ_{00} is 626.7 nm. To augment the cooling effect, we add two cycles that the $a^3\Pi_1(v' = 0) \rightarrow X^1\Sigma^+_{0^+}(v = 1)$ transition is the first vibrational pump and the $a^3\Pi_1(v' = 1) \rightarrow X^1\Sigma^+_{0^+}(v = 2)$ transition is the second vibrational pump. Therefore, two additional lasers with $\lambda_{10} = 686.9154$ nm and $\lambda_{21} = 686.4697$ nm are required.

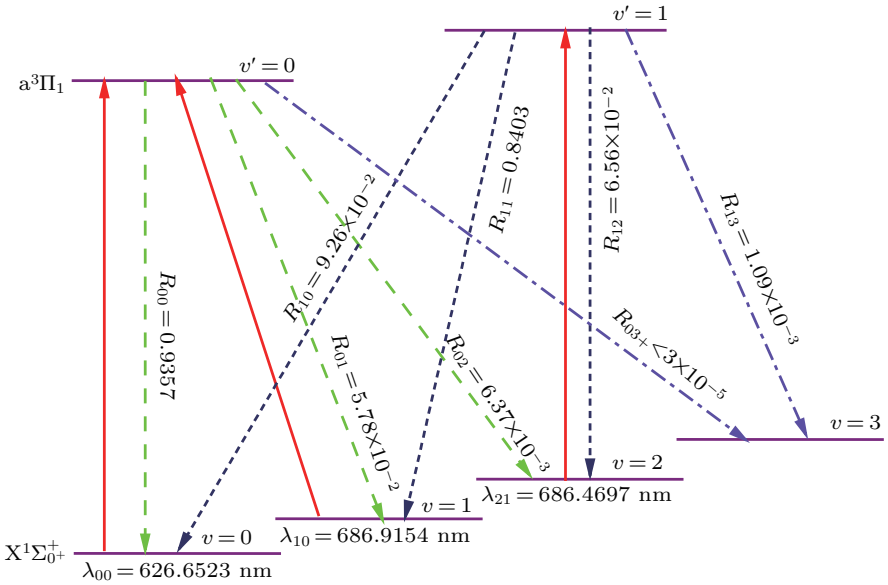


Fig. 5. (color online) The proposed laser-driven transition (solid red) and spontaneous decay (dash line) between the $a^3\Pi_1$ and $X^1\Sigma^+_{0^+}$ states with calculated $R_{v'v}$ for the InH molecule. Here $\lambda_{vv'}$ is the wavelength.

4. Conclusion

The PECs of $X^1\Sigma^+_{0^+}$, $a^3\Pi_{0^-}$, $a^3\Pi_{0^+}$, $a^3\Pi_1$, $a^3\Pi_2$, $A^1\Pi_1$, $1^3\Sigma^+_{0^-}$, and $1^3\Sigma^+_1$ states of InH molecule are investigated at the MRCI+Q level. The AV5Z-DK all-electron basis set for H and ECP28MDF-AV5Z for In atom are chosen. Scalar relativistic corrections are performed using Douglas–Kroll–Hess. The spectroscopic constants (R_e, ω_e, $\omega_e\chi_e$, B_e, D_e, T_e) of the $X^1\Sigma^+$, $X^1\Sigma^+_{0^+}$, $a^3\Pi$, $a^3\Pi_{0^-}$, $a^3\Pi_{0^+}$, $a^3\Pi_1$, $a^3\Pi_2$, $A^1\Pi$, and $A^1\Pi_1$ states are calculated by solving the radial Schrödinger equation using the LEVEL8.2 program from two active spaces. In addition, the calculated result shows that the $A^1\Pi$ state has two potential wells, and the influence of the SOC effects and active space on the PECs is obvious. The comparison between our present work and available experimental data in the literature shows a good agreement.

The PDMs for the $X^1\Sigma^+$, $X^1\Sigma^+_{0^+}$, $A^1\Pi$, $A^1\Pi_1$, $a^3\Pi$, $a^3\Pi_{0^-}$, $a^3\Pi_{0^+}$, $a^3\Pi_1$, and $a^3\Pi_2$ states and the TDMs for the $a^3\Pi_{0^+} \rightarrow X^1\Sigma^+_{0^+}$, $a^3\Pi_1 \rightarrow X^1\Sigma^+_{0^+}$, and $A^1\Pi_1 \rightarrow X^1\Sigma^+_{0^+}$ transitions are obtained based on the MRCI+Q method. On the basis of accurate PECs and TDMs, the theoretical results indicate that the $a^3\Pi_1 \rightarrow X^1\Sigma^+_{0^+}$ transition has highly diagonal branching ratios ($R_{00} = 0.9357$) and suitable radiative lifetime ($\tau = 1.0119 \times 10^{-6}$ s) . These two conditions can ensure rapid and efficient laser cooling of InH molecule. The $a^3\Pi_{0^+} \rightarrow X^1\Sigma^+_{0^+}$ transition is prohibitive to laser cooling because the $a^3\Pi_{0^+} \rightarrow X^1\Sigma^+_{0^+}$ transition has a long radiative lifetime. Concurrently, an optical scheme of three laser cycles with the $a^3\Pi_1 \rightarrow X^1\Sigma^+_{0^+}$ transition to create an ultracold InH molecule is proposed. The main cycling laser wavelength $\lambda_{00} = 626.6523$ nm is determined for the $a^3\Pi_1(v' = 0) \rightarrow X^1\Sigma^+_{0^+}(v = 0)$ transition, and two repumping lasers $\lambda_{10} = 686.9154$ nm and $\lambda_{21} = 686.4697$ nm are chosen for $a^3\Pi_1(v' = 0) \rightarrow X^1\Sigma^+_{0^+}(v = 1)$ and $a^3\Pi_1(v' = 1) \rightarrow X^1\Sigma^+_{0^+}(v = 2)$. These results imply the feasibility of laser cooling of InH.

References

[1] Shuman E S, Barry J F and DeMille D 2010 *Nature* **467** 820
[2] Hellwege K H and Hellwege A M 1974 *Molecular Constants from Microwave, Molecular Beam, and Electron Spin Resonance Spectroscopy* (Berlin: Springer-Verlag)
[3] Kobayashi J, Aikawa K, Oasa K and Inouye S 2014 *Phys. Rev. A* **89** 021401
[4] Molony P K, Gregory P D, Ji Z H, Lu B, Koppinger M P, Le Sueur C R, Blackley C L, Hutson J M and Cornish S L 2014 *Phys. Rev. Lett.* **113** 255301
[5] DeMille D 2002 *Phys. Rev. Lett.* **88** 067901
[6] Ospelkaus S, Ni K K, Wang D, Miranda M H G de, Neyenhuis B, Quemener G, Julienne P S, Bohn J L, Jin D S and Ye J 2010 *Science* **327** 853
[7] Krems R V 2008 *Phys. Chem. Chem. Phys.* **10** 4079
[8] Flambaum V V and Kozlov M G 2007 *Phys. Rev. Lett.* **99** 150801
[9] Hudson J J, Kara D M, Smallman I J, Sauer B E, Tarbutt M R and Hinds E A 2011 *Nature* **473** 493
[10] Isaev T A, Hoekstra S and Berger R 2010 *Phys. Rev. A* **82** 052521
[11] Santos L, Shlyapnikov G V, Zoller P and Lewenstein M 2000 *Phys. Rev. Lett.* **85** 1791

[12] Baranov M A, Dalmonte M, Pupillo G and Zoller P 2012 *Chem. Rev.* **112** 5012

[13] Hummon M T, Yeo M, Stuhl B K, Collopy A L, Xia Y and Ye J 2013 *Phys. Rev. Lett.* **110** 143001

[14] Zhelyazkova V, Cournol A, Wall T E, Matsushima A, Hudson J J, Hinds E A, Tarbutt M R and Sauer B E 2014 *Phys. Rev. A* **89** 053416

[15] Hendricks R J, Holland D A, Truppe S, Sauer B E and Tarbutt M R 2014 *Frontiers in Physics* **2** 51

[16] Tarallo M G, Iwata G Z and Zelevinsky T 2016 *Phys. Rev. A* **93** 032509

[17] Wan M J, Shao J X, Gao Y F, Huang D H, Yang J S, Cao Q L, Jin C G and Wang F H 2015 *J. Chem. Phys.* **143** 024302

[18] Wan M J, Huang D H, Shao J X, Yu Y, Li S and Li Y Y 2015 *J. Chem. Phys.* **143** 164312

[19] Wan M J, Shao J X, Huang D H, Jin C G, Yu Y and Wang F H 2015 *Phys. Chem. Chem. Phys.* **17** 26731

[20] Lane I C 2012 *Phys. Chem. Chem. Phys.* **14** 15078

[21] Kang S Y, Gao Y F, Kuang F G, Gao T, Du J G and Jiang G 2015 *Phys. Rev. A* **91** 042511

[22] You Y, Yang C L, Wang M S, Ma X G and Liu W W 2015 *Phys. Rev. A* **92** 032502

[23] Gao Y F and Gao T 2014 *Phys. Rev. A* **90** 052506

[24] Wells N and Lane I C 2011 *Phys. Chem. Chem. Phys.* **13** 19018

[25] Yang R, Gao Y F, Tang B and Gao T 2015 *Phys. Chem. Chem. Phys.* **17** 1900

[26] You Y, Yang C L, Zhang Q Q, Wang M S, Ma X G and Liu W W 2016 *Phys. Chem. Chem. Phys.* **18** 19838

[27] Grundstrom B 1938 *Nature* **141** 555

[28] Grundstrom B 1939 *Z. Phys.* **113** 721

[29] Garton W R S 1951 *Proc. Phys. Soc., London, Sect. A* **64** 509

[30] Neuhaus H 1958 *Z. Phys.* **150** 4

[31] Neuhaus H 1958 *Z. Phys.* **152** 402

[32] Ginter M L 1963 *J. Mol. Spectrosc.* **11** 301

[33] Ginter M L 1966 *J. Mol. Spectrosc.* **20** 240

[34] Ginter M L 1965 *J. Chem. Phys.* **42** 3222

[35] Ogilvie J F 1992 *Chem. Phys. Lett.* **191** 592

[36] Rajamanickam N, Murali T, Sakthivel T, Gomez M F and Gonzalez J J L 1993 *Collect. Czech. Chem. Commun.* **58** 1491

[37] Zou W l, Lin M R, Yang X Z and Zhang B Z 2003 *Phys. Chem. Chem. Phys.* **5** 1106

[38] Shayesteh A and Ghazizadeh E 2016 *J. Mole. Spec.* **330** 72

[39] Werner H J, Knowles P J, Lindh R, Knizia G, Manby F R and Schütz M 2010 *MOLPRO, version 2010.1, a package of ab initio programs*, see http://www.molpro.net

[40] Laughoff S R and Davidson E R 1974 *Int. J. Quantum Chem.* **8** 61

[41] Knowles P J and Werner H J 1988 *Chem. Phys. Lett.* **145** 514

[42] Werner H J and Knowles P J 1988 *J. Chem. Phys.* **89** 5803

[43] Werner H J and Knowles P J 1985 *J. Chem. Phys.* **82** 5053

[44] Knowles P J and Werner H J 1985 *Chem. Phys. Lett.* **115** 259

[45] Douglas N and Kroll N M 1974 *Ann. Phys.* **82** 89

[46] Hess B A 1986 *Phys. Rev. A* **33** 3742

[47] Le Roy R J 2015 *"LEVEL 8.2: A computer program for solving the radial Schrodinger equation for bound and quasibound levels," Chemical Physics Research Report* CP-668 (University of Waterloo)

[48] Huber K P and Herzberg G 1979 *Molecular Spectra and Molecular Structure IV. Constants of Diatomic Molecules* (New York: Van Nostrand Reinhold Company Inc.)